Interventional Digital Tomosynthesis from a Standard Fluoroscopy System Using 2D-3D Registration with a Reduced Amount of Iodinated Contrast

Mazen Alhrishy[1], Alberto Gomez[1], Andreas Varnavas[1], Tom Carrell[2], Andrew King[1], and Graeme Penney[1].

[1] Dep. of Imaging Sciences and Biomedical Engineering, KCL, London, UK.
[2] Dep. of Vascular Surgery, Guys & St Thomas' NHS Foundation Trust, London, UK.

Abstract. Deboned Interventional Digital Tomosynthesis (de-iDTS) has been recently proposed to enhance vasculature, without the injection of any Iodinated Contrast Medium (ICM), during interventional fluoroscopy. De-iDTS was able to enhance the aortic outline, with much reduced radiation dose compared to Digital Subtraction Angiography (DSA). The injection of ICM in DSA imaging, however, enables much smaller vasculature to be seen. Nevertheless, ICM is nephrotoxic. The aim of this paper is to extend de-iDTS by injecting ICM to enhance small vasculature, such as the renal ostia. Computed Tomography (CT)-based realistic contrast enhanced synthetic fluoroscopy images, were used for de-iDTS reconstruction. De-iDTS images showed that the renal ostia can be clearly seen using only 30% the amount of ICM used in standard DSA imaging. Moreover, de-iDTS images had better Signal Difference to Noise Ratio (SDNR), compared to the synthetic DSA image.

Keywords: interventional digital tomosynthesis, 2D-3D image registration.

1 Introduction

In [1], we proposed an established 2D-3D rigid registration system to reconstruct patient-anatomy-specific 2D Deboned Interventional Digital Tomosynthesis (de-iDTS) images, with much reduced clutter, using standard fluoroscopy system. This was achieved by a C-arm sweep of 40°, to acquire intraoperative fluoroscopy images, which were then registered to the preoperative CT volume. De-iDTS was able to enhance the aortic outline, without the injection of any Iodinated Contrast Medium (ICM), and with much reduced radiation dose compared to Digital Subtraction Angiography (DSA) imaging (an average of -%94 [1]). However, de-iDTS was not able to significantly enhance the renal ostia, which is often the most clinically relevant feature.

In this paper, we extend the method described in [1], by proposing to inject ICM during the C-arm sweep, to enable much smaller vasculature, such as the renal ostia, to be enhanced. The ICM volume we propose to be injected, is much smaller than that used for DSA imaging (e.g. 10-30%). To achieve this, we first developed methods for generating CT-based, realistic, contrast enhanced, synthetic fluoroscopy images, to

simulate a 40° C-arm sweep (i.e. one image per one degree of rotation). These synthetic images were then used to investigate the potential of using a low volume ICM injection during the de-iDTS sweep, to improve renal ostia visualization.

2 Materials and Methods

2.1 Generation of Realistic Contrast Enhanced Synthetic Fluoroscopy Images

Digitally Reconstructed Radiographs (DRRs), are produced by casting rays through the CT volume, and integrating the Hounsfield Units (HU) of voxels along each ray [3]. The voxel HU is related to the linear attenuation coefficient (i.e. μ) of that voxel by $HU = 1000 \times (\mu - \mu_w)/\mu_w$, where μ_w is the linear attenuation coefficient of water. The process of producing a DRR image, resembles the process of projecting X-rays through a medium to produce a fluoroscopy image. Assuming a monoenergetic beam of X-rays, the relationship between the intensity of the incident X-ray on the image detector (I_d), and the travelled distance $\int dz$ through a medium, which has a linear attenuation coefficient $\mu(z)$, is described by Lambert-Beer law $I_d = I_0 exp(-\int \mu(z)dz)$, where I_0 is the initial X-ray intensity. The HU and Lambert-Beer equations can be combined to relate I_d to the integral of HUs along the ray path, such as:

$$I_d = I_0 exp(-\int (\frac{HU(z)\mu_w}{1000} + \mu_w)dz) \tag{1}$$

Typically, I_d is logarithmically transformed prior to image processing and visualization [2, 4]. Therefore, we assume a logarithmic relationship between the final fluoroscopy image (I_{fl}) and I_d (i.e. $I_{fl} \propto \log(I_d)$). Under this assumption, we can write that $I_{fl} \propto \int HU(z)dz$, which shows that I_{fl} is linearly related to the integral of HUs along the ray path, and thus linearly related to the produced DRR at the registration position. Nevertheless, the above equations assume that the CT and I_{fl} are both acquired using the same X-ray spectrum, which is not usually true. Therefore, the ratio of the linear attenuation coefficient of bone to soft-tissue will usually vary dependin on the X-ray spectrum used. As a result, the produced DRR image will have a different bone to soft-tissue contrast, compared to I_{fl}. To account for the X-ray spectrum differences to produce a realistic synthetic I_{fl}, we took a similar approach to [5], which involves segmenting the CT volume into bone, soft-tissue, and vessels, before generating three DRR images, one for each segmentation. Therefore, we can linearly relate I_{fl} with the produced DRRs from bone (DRR_b), soft-tissue (DRR_t), and vessels (DRR_v), as in:

$$I_{fl} = a_b DRR_b + a_t DRR_t + a_v DRR_v + b \tag{2}$$

This equation can be solved using linear least square fitting, however, because I_{fl} contains no ICM, a_v will have zero value. Therefore, we use a clinical angiography image (I_{ang}) instead of I_{fl}, to solve (2).

Figure 1 illustrates the method to generate CT-based synthetic images. The process can be split up into five steps:

I. The preoperative CT volume (a) was registered to I_{ang} (d), using the 2D-3D registration described in [1] (i.e. calculating the transformation M_{ang}, which determines the

view position of I_{ang} with respect to the CT volume coordinate system). The registration accuracy and roubstness have been previously validated in [3].

II. The CT volume was segmented into bone (CT_b), soft-tissue (CT_t), and vessels (CT_v) (b1,b2, and b3, respectively). To acheive this, the semi-automatic segmentation tool available in ITK-SNAP [7], was used to segment bone (HU $\geq$ 200) and the aorta, to produce CT_b and CT_v, respectively. Then, both segmentations were excluded from the CT volume to produce CT_t. Excluded voxels were set to zero.

III. A DRR was produced from each segmentation at the registration position: DRR_b, DRR_t, and DRR_v (c1,c2, and c3, respectively). All DRRs were generated as described in [1] (i.e. by casting rays through the CT segmentations using M_{ang}).

IV. Two Regions of Interest (ROIs) were chosen within I_{ang}. ROI_1 included parts of the vessels where ICM was most homogeneous (marked with white dashed-lines). ROI_2 included ROI_1, bone, and soft-tissue, but no interventional devices (marked with white solid-lines). Equation (2) was then solved within the two ROIs, using linear least square fitting, as follows:

$$I_{ang}^{ROI_2} = a_b DRR_b^{ROI_2} + a_t DRR_t^{ROI_2} + a_v DRR_v^{ROI_1} + b \tag{3}$$

V. The calculated coefficients and the DRR images were used to produce the following four Synthetic Images (SIs):

1. One synthetic fluoroscopy image: $SI_{0\%}$, where $a_v = 0$ was used.
2. Three synthetic angiography images: $SI_{10\%}$, $SI_{20\%}$, and $SI_{30\%}$, where 10%, 20%, and 30% the value of a_v was used to simulate 10%, 20%, and 30% the amount of ICM used in standard DSA imaging, respectively.

2.2 Introducing Soft-Tissue Motion and Quantum-Noise

For realistic simulation, soft-tissue motion was introduced, at each view position in the simulated 40° C-arm sweep, before de-iDTS reconstruction. This was accomplished, by deforming the generated DRR_t image, at each view position, by different amounts, before producing the SIs. The DRR_t image was deformed using a random smooth vector field, generated from a uniform cubic B-spline grid. The B-spline grid parameters, and the mean and maximum displacements, were set so that, the simulated deformation resembles the deformation caused by the intestinal peristaltic motion. This was achieved, by observing this deformation in a time-sequence fluoroscopy image, and setting the B-spline grid spacing to be equal to the average diameter of features from the large intestine, and for the maximum deformation magnitude to be equal to the average magnitude of bowel motion.

Quantum-noise is the primary source of noise in low dose X-ray images. Other sources of noise exist in the imaging system, but can be ignored [2]. Quantum-noise would still exist at high dose imaging, because of the quantum nature of X-ray. However, by increasing the dose, photon fluctuations decrease as the average number of photons reaching the detector increases. Prior to de-iDTS reconstruction, quantum-noise was added to the SIs, after introducing soft-tissue motion at each view position in the simulated 40° C-arm sweep. Quantum-noise was generated directly from the images, where each pixel intensity was interpreted as the mean of a Poisson distribution.

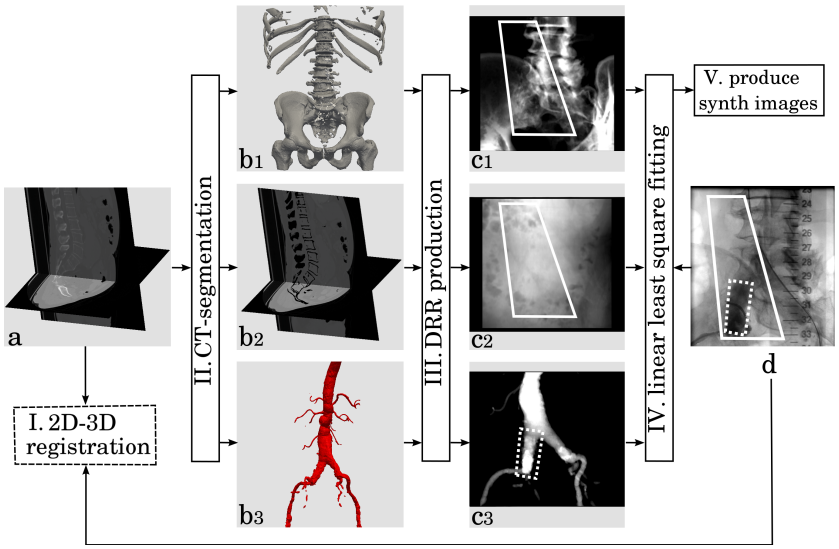

Fig. 1. a) The CT volume is registered to d) the angiography image (I_{ang}), and then segmented into bone (b1), soft-tissue (b2), and vessels (b3). The segmentations are used to produce 3 DRRs at the registration position (c1, c2, and c3). The DRRs and I_{ang}, are input into a linear least square fitting program, which employs ROI_1 (marked with white dashed-lines) and ROI_2 (marked with white solid-lines), to calculate the linear coefficients, which are finally used to produce SIs.

3 Data and Experiments

The following data from a patient who underwent an endovascular aneurysm repair, was employed: 1) The preoperative CT scan, with voxels size of $0.77\,\text{mm} \times 0.77\,\text{mm} \times 0.80\,\text{mm}$. 2) 40 view positions of the C-arm, which were obtained as described in [1]. This involved rotating the C-arm $\pm 20^\circ$ right-left anterior oblique to acquire a time-sequence of images, with pixels size of $0.216\,\text{mm} \times 0.216\,\text{mm}$. These images were registered to the CT volume to calculate the transformation matrices, which were sampled to one view position per one degree of rotation (i.e. $M_i = PR_iT_i$, $i = 1,\ldots,40$). 3) An angiography image (I_{ang}), produced from an angiography time-sequence, acquired with pixels size of $0.216\,\text{mm} \times 0.216\,\text{mm}$.

3.1 Simulation and Reconstruction Experiments

The CT scan, and the produced I_{ang}, were used to calculate the linear coefficients (steps I-IV in Sec. 2.1). Then, for each of the 40 view positions of the C-arm, DRR_b, DRR_t, and DRR_v were generated (step III in Sec. 2.1), and combined with the calculated linear coefficients to produce $SI_{0\%}$, $SI_{10\%}$, $SI_{20\%}$, and $SI_{30\%}$ (step V in Sec. 2.1).

A curved reconstruction surface in the CT volume was produced, along the midline of the aorta and renal arteries, and used for reconstruction, as described in [1]. Four de-iDTS images were reconstructed, from an Anterior-Posterior (AP) view (i.e. the chosen

target image had an AP view), before and after adding soft-tissue motion and quantum-noise. These were: de-iDTS (using the 40 $SI_{0\%}$), de-iDTS1 (using the 40 $SI_{10\%}$), de-iDTS2 (using the 40 $SI_{20\%}$), and de-iDTS3 (using the 40 $SI_{30\%}$).

3.2 Validation Experiments

A synthetic DSA image was produced using a 100% simulated ICM, at the target view position for comparison (SI_{DSA_T}). Soft-tissue motion and quantum-noise were then introduced to SI_{DSA_T}, as explained in Sec. 2.2. Signal Difference to Noise Ratio (SDNR), was used as a measure of feature's detectability. Two Profile Lines (PLs), were manually positioned across the left and right renal ostia in the produced SI_{DSA_T}, before adding soft-tissue motion and quantum-noise (Fig. 3.a1). Foreground (FG) and background (BG) regions were then automatically delineated, using the full width half maximum method, and SDNR was caculated as per [6] ($SDNR = (\bar{I}_{FG} - \bar{I}_{BG})/\sigma_{BG}$, where $\bar{I}_{FG}$ and $\bar{I}_{BG}$ are the mean normalized intensities of FG and BG regions, respectively, and σ_{BG} is the standard deviation of BG intensities). SDNR calculations were repeated after soft-tissue motion and quantum-noise were introduced to SI_{DSA_T}. Finally, PL1 and 2, were placed at the same positions inside de-iDTS1, de-iDTS2, and de-iDTS3, and SDNR calculations were repeated, before and after adding soft-tissue motion and quantum-noise.

4 Results

In Fig. 2, we show for visual comparison: a) a clinically acquired fluoroscopy image at the target view position, and b) the generated SI at the same view position, after adding motion and noise artefacts, with %30 simulated ICM (i.e. $SI_{30\%_T}$). Both 'c' and 'd' also show $SI_{30\%_T}$, however, c) shows the effect of bone removal, and d) shows the effects of introducing soft-tissue deformation, and quantum-noise. The simulated ICM in 'b', cannot be distinguished from the overlaying high contrast vertebrae, but can be seen in 'c', after removing the vertebral bone. In 'd', the same part of the bowel is highlighted with a white contour, before and after introducing deformation, to illustrate the magnitude of soft-tissue motion introduced. In addition, in 'd', a ROI is magnified before (white box with solid-lines), and after (white box with dashed-lines) adding quantum-noise, to show the effect of introducing quantum-noise.

Figure 3 shows a ROI around the renal ostia in: a) SI_{DSA_T}, b) de-iDTS, c) de-iDTS1, d) de-iDTS2, and e) de-iDTS3, before adding soft-tissue motion and quantum-noise (1), and after adding soft-tissue motion (2), and quantum-noise (3). The 100% contrast SI_{DSA_T} images (a1,2,3), clearly show the renal ostia, but the effects of motion (a2), and noise (a3) can be seen to reduce clarity. The zero contrast de-iDTS images (b1,2,3), show part of the renal outline, but not the renal ostia. In the de-iDTS images with contrast (c,d,e), the renal ostia can be seen, clarity improves as contrast is increased from 10% (c) to 30% (e), and is degraded by the introduction of motion and noise. However, even with only 30% contrast, good depiction of the renal ostia is shown, even with inclusion of motion and noise (e3).

Figure 4 shows a scatter plot of the calculated SDNR values. It can be seen that SDNR values (crosses) decreased for all images after introducing motion (triangles),

and decreased further after adding noise (circles). However, for SI_{DSA_T}, the percentage decrease was much more substantial when compared to de-iDTS results, due to motion and noise artefacts (for example, PL1 SDNR value decreased by -41.49% after introducing motion, and -60.67% after adding noise for SI_{DSA_T}; whereas it only decreased by -2.31% and -5% for de-iDTS3). Therefore, even though SI_{DSA_T} had the highest SDNR values before adding motion and noise, SI_{DSA_T} scored the lowest SDNR values, compared to all other images, after adding motion and noise.

5 Discussion

Reconstruction results, after adding soft-tissue motion and quantum-noise, showed that the renal ostia can be clearly seen with added synthetic contrast to simulate 30% of the ICM amount used in standard DSA imaging. The synthetic contrast was added homogeneously, inside the entire aorta, during the simulated C-arm sweep. However, clinical angiography images contain contrast only in some parts of the aorta, after the injection of an ICM bolus. If an ICM bolus is injected during the 40° C-arm sweep, the de-iDTS image will be reconstructed from images containing partial ICM in the aorta. Thus, to ensure that all images of the sweep contain ICM in the entire aorta, a slow constant injection of ICM is required, during the duration of the sweep. This might however, require more ICM injection than what was estimated (i.e. >30%), as the C-arm sweep takes currently around 8 sec on average. Nevertheless, if the de-iDTS technique became incorporated with the fluoroscopy system, where only one image per one degree of rotation is acquired, at a high frame rate, the C-arm sweep will take a shorter time (e.g. if images are acquired at 10 frame per sec, the sweep will take around 4 sec depending on the C-arm speed limitation). The produced synthetic DSA image (SI_{DSA_T}), with motion and noise artefacts (Fig. 3.a3), was of much better quality compared to clinical DSA images. This is because unlike clinical angiography images, the employed synthetic angiography images to produce SI_{DSA_T}, contained simulated contrast in the entire aorta. Nevertheless, SI_{DSA_T} with motion and noise artefacts, had the lowest SDNR values compared to de-iDTS images. This is due to the fact that DSA images are subtraction images, therefore DSA will be greatly effected by differences between the mask and contrast images, which are caused by effects other than contrast (e.g. motion and noise). Whereas de-iDTS images, are created by averaging intensities from all the input images, and is able to average out noise and motion effects, if they are of random nature.

6 Conclusions

Using realistically generated synthetic data, we have investigated the feasibility of using interventional digital tomosynthesis imaging, together with low volume ICM injection, to produce de-iDTS angiographic images. Results show that de-iDTS image quality is affected to a much lesser extent than DSA images by image artefacts caused by noise or bowel motion. Results also showed that when bowel motion and noise were present, de-iDTS images produced with 30% contrast were of better quality than DSA images produced with 100% contrast.

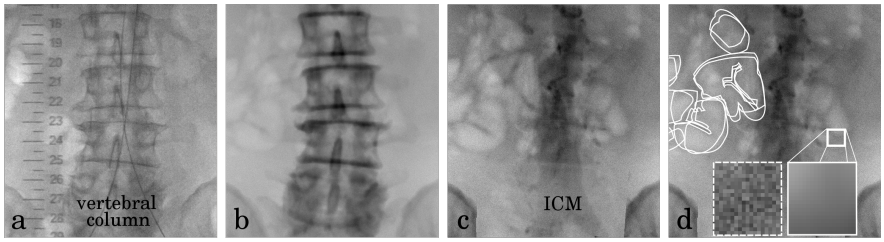

Fig. 2. a) a clinical I_{fl_T} acquired at the target view position, b) $SI_{30\%_T}$ produced at the same view position after adding motion and noise artefacts. 'c' and 'd' also show $SI_{30\%_T}$, however, c) shows the effect of bone removal, and d) shows the effects of introducing deformation and noise.

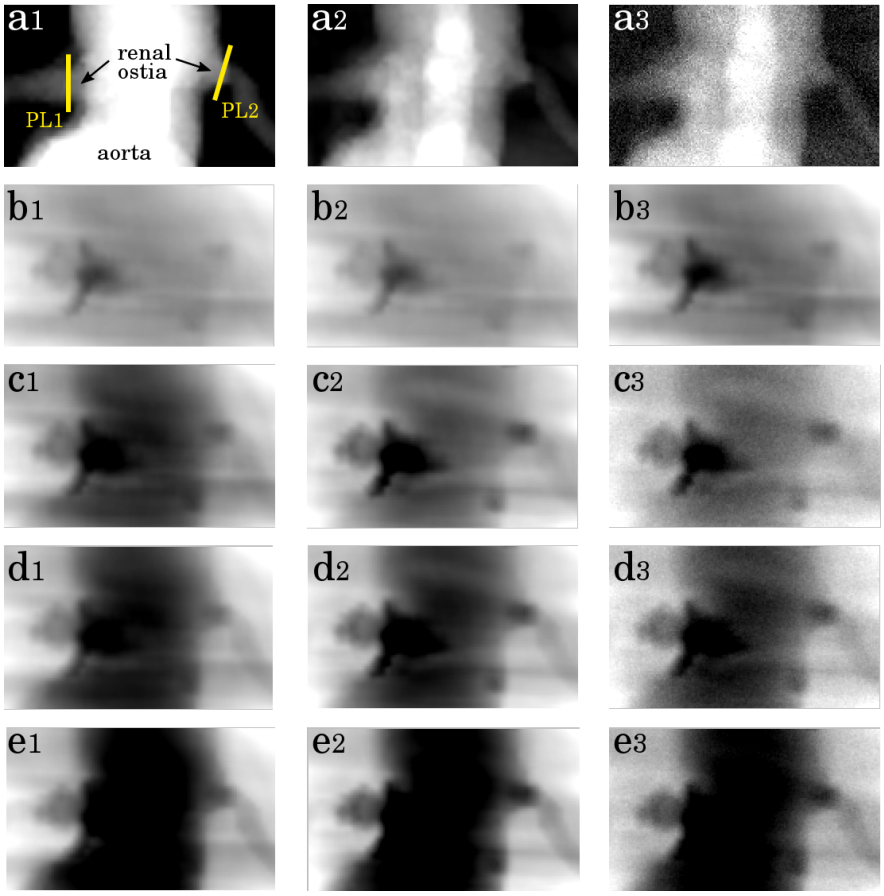

Fig. 3. a) SI_{DSA_T}, b) de-iDTS, c) de-iDTS1, d) de-iDTS2, and e) de-iDTS3, before adding motion and noise (1), and after adding motion (2) and noise (3). 'a1' shows PLs positions.

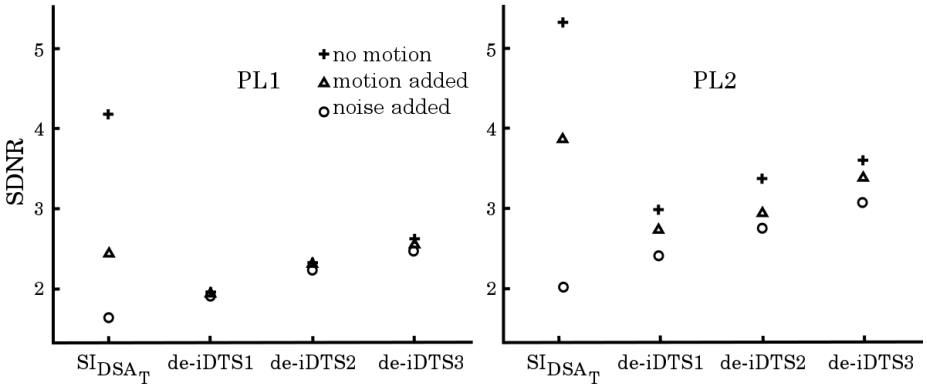

Fig. 4. Plot of calculated SDNR values for visual comparison, for PLs 1 and 2.

References

1. Alhrishy, M., Varnavas, A., Carrell, T., King, A., Penney, G.: Interventional digital tomosynthesis from a standard fluoroscopysystem using 2D-3D registration. Med Image Anal 19(1), 137–148 (2015)
2. Hensel, M., Pralow, T., Grigat, R.R.: Modeling and real-time estimation of signal-dependent noise in quantum-limited imaging. In: Proc. of the 6th WSEAS int conf. pp. 183–191. ISPRA'07 (2007)
3. Penney, G., Batchelor, P., Hill, D., Hawkes, D., Weese, J.: Validation of a two-to three-dimensional registration algorithm for aligning preoperative CT images and intraoperative fluoroscopy images. Medical Physics 28, 1024 (2001)
4. Tobis, J.M., Nalcioglu, O., Henry, W.L.: Digital subtraction angiography. Chest Journal 84(1), 68–75 (1983)
5. Walsum, T.V., Zuiderveld, K.J., Chin-A-Woeng, J.W.C., Eikelboom, B.C., Viergever, M.A.: CT-based simulation of fluoroscopy and DSA for endovascular surgery training. In: CVRMedMRCAS'97. vol. 1205, pp. 273–282. Springer (1997)
6. Wu, T., Moore, R.H., Rafferty, E.A., Kopans, D.B.: A comparison of reconstruction algorithms for breast tomosynthesis. Med Phys 31, 2636 (2004)
7. Yushkevich, P.A., Piven, J., Hazlett, H.C., Smith, R.G., Ho, S., Gee, J.C., Gerig, G.: User-guided 3D active contour segmentation of anatomical structures: significantly improved efficiency and reliability. Neuroimage 31(3), 1116–1128 (2006)